

Periodic temporal environmental variations induce coexistence in resource competition models

Tom Burkart¹ and Erwin Frey^{1, 2, *}

¹Arnold Sommerfeld Center for Theoretical Physics and Center for NanoScience, Department of Physics, Ludwig-Maximilians-Universität München, Theresienstraße 37, D-80333 München, Germany

²Max Planck School Matter to Life, Hofgartenstraße 8, D-80539 München, Germany

(Dated: February 24, 2022)

Natural ecosystems, in particular on the microbial scale, are inhabited by a large number of species. The population size of each species is affected by interactions of individuals with each other and by spatial and temporal changes in environmental conditions, such as resource abundance. Here, we use a generic population dynamics model to study how, and under what conditions, a periodic temporal environmental variation can alter an ecosystem's composition and biodiversity. We demonstrate that using time scale separation allows one to qualitatively predict the long-term population dynamics of interacting species in varying environments. We show that the notion of *competitive exclusion*, a well-known principle that applies for constant environments, can be extended to temporally varying environments if the time scale of environmental changes (e.g., the circadian cycle of a host) is much faster than the time scale of population growth (doubling time in bacteria). When these time scales are similar, our analysis shows that a varying environment deters the system from reaching a steady state, and coexistence between multiple species becomes possible. Our results posit that biodiversity can in parts be attributed to natural environmental variations.

I. INTRODUCTION

In a healthy ecosystem, a wide variety of species coexist, interacting with each other through cooperative or competitive behavior [1, 2]. These interactions tend to be complex and entangled: the causal chain between a modification of the ecosystem and the corresponding observable effects, in particular on the biodiversity, are not always obvious [3–5]. To describe how the population sizes of interacting species change over time for specific systems, various models have been developed (for a comparison, see, for example, Ref. [6]). Among those, the Monod model [7] is presumably the most widely used model, as it includes the effect of growth-restricting parameters (usually a limiting resource) in the model.

Only few models, however, account for the fact that the vast majority of ecosystems occurring in nature are subject to an external temporal structure, such as light availability during day-night cycles [8], temperature variations during the change of the seasons [9], or the circadian rhythm of vertebrate gut microbiota [10], despite accumulating evidence that organisms are strongly affected by such external temporal variations. For example, recent experiments on the fungus *Neurospora crassa* showed that gene expression can be coupled to periodic temperature variations (entrainment) [11]. Furthermore, knock-out experiments on the bacterium *Rhodopseudomonas palustris* identified a protein that enhances cell growth when exposed to light-dark cycles, but does not provide any advantage in constant environments [12]. On the level of microbial communities, it was shown that the

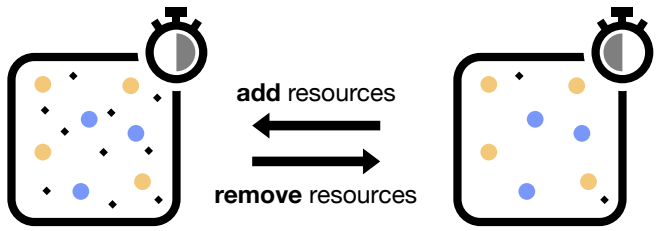


Figure 1. (Color online) Illustration of the resource competition model with periodically switching resource abundance. Yellow (or light gray) and blue (or gray) balls represent individuals of distinct species. Diamonds indicate available resource units. For a fraction of each period, an abundant amount of resources are available (left). For the remainder of the period, few or no resources are available (right), inhibiting the growth of the populations.

composition of the mouse gut microbiome varies synchronized with the externally imposed day-night cycle [13], and that the overall biodiversity is affected by a time-restricted feeding schedule [14].

Theoretical models for population dynamics that consider external temporal structures mainly investigate the growth dynamics of a single population [15–25], or study the interactions between multiple populations for fairly specific biological systems [8, 24, 26–35], with recently increased focus on stochastically varying environments [36–42]. These existing approaches show how populations change over time in specific systems; however, as they are often tailored to a certain biological application, they cannot be applied in general to understand how interacting populations are affected by a varying environment, especially in terms of their long-term ability to coexist. Thus, how can a periodic temporal structure in general

* frey@lmu.de

alter an ecosystem's ability to sustain or enhance biodiversity?

To address this question, we study a simple yet fairly general growth model that forbids coexistence in a constant environment according to the competitive exclusion principle [43, 44]. We focus on the qualitative differences that appear when the environment is made explicitly time-dependent. Our analysis reveals a mechanism by which the competitive exclusion can be overcome by periodically changing the environment for a system hosting two species [Fig. 1]. Insights gained by studying the competitive behavior of two species often help elucidating how a community involving more than two species behaves [45, 46]. Our analysis demonstrates that the qualitative population dynamics of a ecosystem consisting of more than two distinct competing species in a time-dependent environment can be predicted from the pairwise interactions between the species.

This paper is structured as follows: We start in Section II by introducing a resource competition model, which is used as an example throughout this paper, along with a generalized growth model. We discuss the most important features of the generalized model and the implications of the competitive exclusion principle in a time-independent environment. In Section III, we study a system with two competing species that are subject to a periodic modulation of the environment, which is accounted for via a time-dependent resource abundance. Finally, we extend the analysis to systems with more than two species, and study how a general external temporal pattern impacts a more diverse ecosystem in Section IV. We conclude with a concise summary and an outlook.

II. MODEL

Consider a population with M distinct species, each with a population size $n_i(t)$, $i \in \{1, \dots, M\}$. Population growth is assumed to follow the Monod model [7], with a maximum per-capita growth rate μ_i . All species, totalling a population size of $N(t) = \sum_i n_i(t)$, uniformly feed on and compete for a single common abiotic resource S . The term "abiotic" refers to the resource abundance being constant or having an externally imposed time dependence, rather than being a dynamic quantity. The resource is assumed to be replenished immediately after it is consumed, such that the limiting factor for population growth is the amount of *unbound* resources $S - N(t)$. The impact of resource scarcity is quantified by the species-dependent carrying capacities K_i [43]. Furthermore, the population size of each species is assumed to decrease at a per-capita rate δ_i . Altogether, the dynamics of the population sizes are described by the following chemostat model [47, 48]:

$$\frac{d}{dt} n_i(t) = n_i(t) \cdot \left(\mu_i \frac{S - N(t)}{S - N(t) + K_i} - \delta_i \right). \quad (1)$$

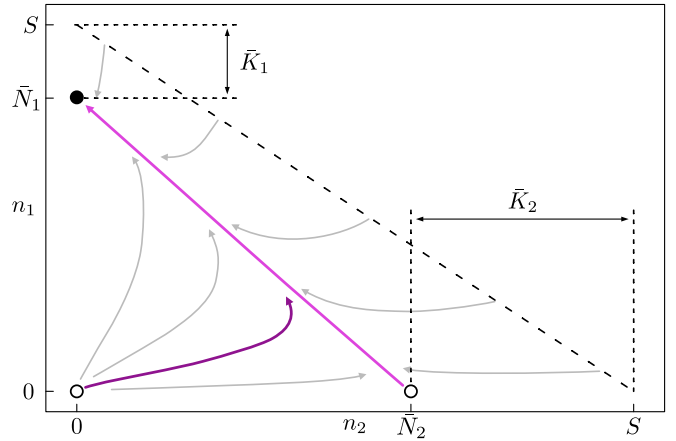


Figure 2. (Color online) Representative flow diagram showing the time evolution of the population sizes of two competing species. The dashed line represents a subspace of constant total population size $N = S$. Light gray arrows indicate the overall flow. The pink (or gray) trajectory represents the heteroclinic orbit connecting the two non-trivial fixed points. For two competing species, there are one stable (filled circle) and two unstable fixed points (open circles). Following the competitive exclusion principle, the stable fixed point corresponds to the species with the smallest resource buffer \bar{K}_i . The purple (dark gray) line represents a specific trajectory initially favoring the species with larger resource buffer, but finally resulting in the survival of the species with the smaller resource buffer, following the competitive exclusion principle.

Due to the limited resource availability, each species i has a maximally sustainable total population size \bar{N}_i at which the population growth is exactly levelled by decay. This population size is given by $\bar{N}_i = S - \bar{K}_i$, where the offset \bar{K}_i can be interpreted as a *resource buffer*, denoting the amount of resources that a species i leaves unbound when reaching the steady state [Fig. 2]; derivation in Appendix VII A. Note that the index i in the symbol \bar{N}_i refers to the fact that the population n_i can not grow if the total population size is larger than the maximally sustainable population size of species i , i.e., if $N > \bar{N}_i$; a different species j may still grow at this total population size if $\bar{N}_j > \bar{N}_i$. In the chemostat model, when a species does not face competition, this maximally sustainable total population size \bar{N}_i is equal to the steady state population size n_i^* (fixed point).

A. The competitive exclusion principle

In a system hosting two or more distinct species whose population dynamics are described by Eq. (1), competition for the limiting resource will allow only one survivor, namely the one with the smallest resource buffer \bar{K}_i . This rule is known as the *competitive exclusion principle* [43, 44]. It can be understood heuristically in the following way: For two competing species, both populations can grow until the total population size N approx-

imately matches the maximally sustainable population size \bar{N}_i of one of the two species (purple or dark gray) flow line in Fig. 2 approaching the heteroclinic orbit). At this point, the net growth for this species is zero, whereas the other species (the one with the smaller resource buffer) can still grow, thereby further increasing the total population size. Since this reduces the amount of resources available to the species with the larger resource buffer, its population size will start to decrease, eventually leading to extinction of the species with the larger resource buffer (flow along the heteroclinic orbit towards the stable fixed point in Fig. 2).

In total, a system hosting two species therefore has three fixed points: assuming $\bar{K}_1 < \bar{K}_2$, the stable fixed point is located at $(n_1, n_2) = (\bar{N}_1, 0)$, whereas the two unstable fixed points are located at $(0, \bar{N}_2)$ and $(0, 0)$. The stable and unstable fixed points are represented as filled and open circles in Fig. 2, respectively. If the system consists of more than two species, this recursive argument can be repeated to show that the species with the lowest resource buffer will be the only one to survive [47].

An interesting feature of the competitive exclusion principle is that the outcome solely depends on the resource buffer, but not explicitly on the growth rates of the populations [48, 49]. Figure 2 illustrates that a species growing quickly at high resource abundance is still suppressed in the long run by another species that grows more slowly, but has a smaller resource buffer. A key prediction of the chemostat model, Eq. (1), is that the most successful strategy for surviving in competition with other species is to minimize one's resource buffer \bar{K}_i , i.e. to optimize one's resource utilization.

B. The non-autonomous chemostat model

This prediction of the chemostat model only applies in an ecosystem that has no external temporal structures, so that all model parameters remain constant in time, referred to as an *autonomous* system. In fact, it has previously been shown that introducing an external temporal structure to the chemostat model can lead to qualitatively different results [8, 48]. In the following, we incorporate such a temporally varying environment in the chemostat model by allowing the abiotic resource S to switch periodically between two values. Thus, the differential equations describing the population dynamics become *non-autonomous*. In principle, any of the model parameters may depend on time, and one could also arrive at the following results using a time dependence other than the resource abundance; see for example Refs. [33, 39, 48, 50]. However, it is more illustrative and biologically relevant [8, 51] to study the case where the resource varies over time.

To derive the non-autonomous variant from the autonomous chemostat model, Eq. (1), we replace the constant resource abundance S with a time-dependent $S(t)$. For simplicity, we assume that $S(t)$ switches periodically

between two constant values S and S' , with a period duration of T . To further simplify the analysis, we explain the effect of an externally imposed time dependence for the case $S' = 0$ first, and generalize to $0 \leq S' < S$ later. The time window where resources are abundant ($S(t) = S$) is assumed to last a proportion νT of the total period, with the *activity ratio* $\nu \in [0, 1]$. For the remainder of the total period, $(1 - \nu) T$, resources are assumed to be scarce ($S(t) = S'$). If no resources are available, then there should be no growth. This is made explicit in the chemostat model by only allowing non-negative values of the unbound resources ($S(t) - N(t)$). The resulting differential equation including the time-dependent resource $S(t)$ reads

$$\frac{dn_i(t)}{dt} = n_i(t) \left[\mu_i \frac{\max(S(t) - N(t), 0)}{\max(S(t) - N(t), 0) + K_i} - \delta_i \right], \quad (2a)$$

$$S(t) = \begin{cases} S & \text{for } 0 \leq t < \nu T, \\ S' & \text{for } \nu T \leq t < T, \end{cases} \quad S(t+T) = S(t). \quad (2b)$$

This non-autonomous chemostat model will serve as an example to illustrate the results throughout this paper. Within each time period T , there are therefore two distinct phases: While resources are abundant, the populations grow just as in the autonomous chemostat model, Eq. (1). This growth is impeded while resources are scarce, and in the special case $S' = 0$ that will be investigated first the population sizes decay exponentially.

C. General model class

The chemostat model is a special case of a general class of growth models referred to as *competing species models* [52, 53]. In this class of models, the net per-capita growth rates are general growth functions $f_i(\{n_j(t)\}, t)$ for each species i . The term ‘competing’ implies that the growth rates decrease for increasing population sizes, $\partial_{n_j} f_i(\{n_j(t)\}, t) \leq 0$.

When the population growth depends on a linear combination of the individual population sizes $\sum_j \alpha_j n_j$, the growth functions f_i can be rewritten in terms of the total population size N . This can be achieved by rescaling the population sizes by their relative weighting factor α_j . The resulting class of models defined by

$$\frac{d}{dt} n_i(t) = n_i(t) \cdot f_i(N(t), t), \quad (3a)$$

$$\frac{\partial}{\partial n_j} f_i(N(t), t) \leq 0 \quad (3b)$$

is a generalization of the non-autonomous chemostat model in Eq. (2). Additional constraints to make the growth functions f_i realistic are stated in Appendix VII B. We will show that the concepts that can lead to increased biodiversity in the resource competition model can actually be applied to the entire class of competing species models as specified in Eq. (3).

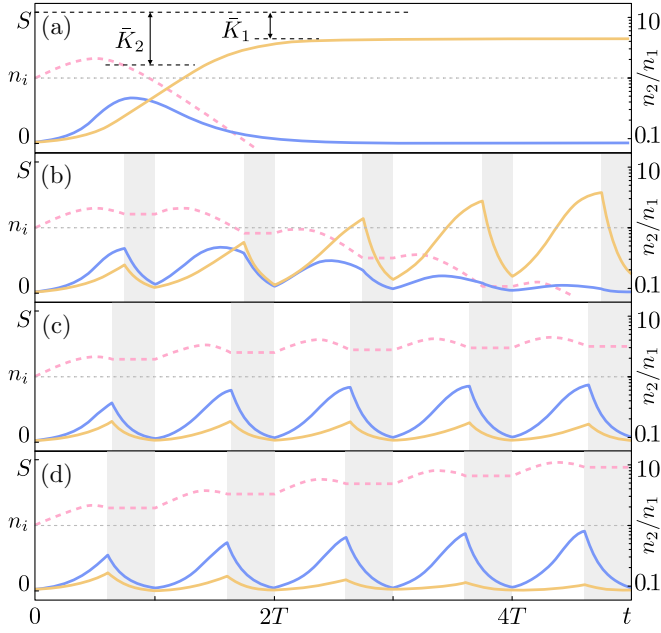


Figure 3. (Color online) Comparison of the population dynamics at a fixed periodicity $T = 7$ for four different fractions νT with resources available: (a) $\nu = 1$, (b) $\nu = 0.75$, (c) $\nu = \nu_u \approx 0.64$, and (d) $\nu = 0.61$ (remaining parameters in Table I). Gleaner (n_1) population sizes are shown in yellow (or light gray), the opportunist (n_2) is shown in blue (or gray). Dashed lines show the relative population size $n_2(t)/n_1(t)$ (log scale, right axis). Shaded regions indicate time periods when resources are scarce. In the time-independent case (a), competitive exclusion takes its full effect, with the opportunist approaching its steady state at $S - \bar{K}_2$ quickly, but being overtaken by the gleaner with the smaller resource buffer \bar{K}_1 eventually. These dynamics are altered for time-dependent environments: For increasingly long time episodes without resources, competitive exclusion becomes less effective (b), eventually leading to coexistence (c), or even to inverted dynamics (d). Whether the external temporal pattern leads to regular dynamics, inversion, or coexistence, depends on the duration of the period with resources absent, which is parametrized by the activity ratio ν .

III. TWO-SPECIES COMPETITION

In this section we begin the analysis of the role of time-dependent resources with a discussion of systems hosting two competing species. For simplicity we assume that the decay rates δ_i are identical for both species, which is a basic feature of chemostat models where the decrease in each species' population size is mainly due to washout from the chemostat [48].

A. Reversal of survival

In a time-independent environment, the competitive exclusion principle predicts which species will survive

when the total population size reaches the maximally sustainable population size; the population size of this surviving species (termed *gleaner*) will be labeled by n_1 in the following. While the gleaner species will dominate in the long run for high total population sizes, the other species (termed *opportunist*, n_2) may grow faster on short time scales, as shown in Fig. 3a. Such a scenario, known as *gleaner-opportunist trade-off* [47], has been observed, for example, in phytoplankton competition [8].

In contrast to the time-independent case, the opportunist can gain a significant advantage from the quick growth at low total population sizes in an environment with periodically switching resources: While resources are available and before the opportunist's population size can reach its maximum, the fast growth of the opportunist ensures that the relative population size $n_2(t)/n_1(t)$ increases to the advantage of the opportunist (dashed lines in Fig. 3). During the time period when resources are absent, both population sizes decrease, but the relative population size remains the same since we assumed equal decay rates δ_i here. Note that, if this time period without resources is short enough, then the total population size remains high and the gleaner is not affected critically by the lack of resources, so that the opportunist loses to the gleaner in the long run [Fig. 3b]. In contrast, for a sufficiently long time period without resources, the populations are set back to very low population sizes each period. Due to the fast growth of the opportunist at low total population sizes, the opportunist can take over in the long run, whereas the gleaner will go extinct, which is the *inverse* result compared to the competitive exclusion principle [Fig. 3d]. At the transition from short to long time periods without resources, the opportunist's advantage at low population sizes and the disadvantage at high population sizes level each other, leading to *coexistence* between the gleaner and the opportunist [Fig. 3c].

B. Bifurcation diagram: inversion & coexistence

Under what conditions will the opportunist species survive instead of the gleaner species? Heuristically, there are three conditions on the time dependence of the resource abundance that must be met for this reversal of survival to occur: (i) The time window during which resources are available needs to be short enough so that competitive exclusion does not take effect. (ii) The time window during which resources are absent needs to be long enough to ensure that the total population size decays to a small value before the resources become available again. (iii) The time window during which resources are available needs to be long enough so that the populations can recover from the time window where resources are absent, as otherwise all populations would go extinct over the course of multiple periods. These requirements impose constraints on the activity ratio ν that characterizes the external temporal structure.

In the following, we provide quantitative reasoning for these qualitative arguments. To this end, we approximate the continuous dynamics with time-dependent resource abundance by a discrete equivalent (a map) with time-independent resource abundance. Based on this approximation, we generalize the competitive exclusion principle to time-dependent environments. From this, we then derive the constraints on the activity ratio for reversal of survival, validating the arguments above and allowing to estimate the bifurcation diagram for the long-term population dynamics.

1. Approximation of the population dynamics

In the following, we study the population dynamics in the competing species model class with externally imposed time dependence, as specified in Eq. (3). Now, assume that nonlinear contributions to the population size changes $\partial_t n_i(t)$ within a single period T can be neglected. This assumption is reasonable if the population size remains approximately constant over the course of a single period T , meaning that $n_i(t) \approx n_i(k \cdot T)$ for $t \in [kT, (k+1)T]$. In Appendix VII C, we show that this is valid for period durations T short compared to the time scales of growth, $T \ll f_i^{-1}$.

Using this approximation and writing $n_{i,k} := n_i(k \cdot T)$ and $N_k := N(k \cdot T)$ to denote the population size after k periods, one can approximate the continuous population dynamics in Eq. (3) by a discrete map:

$$\begin{aligned} n_{i,k+1}(\{n_{j,k}\}) &= n_{i,k} \cdot \exp \left[\int_0^T dt f_i(N_k, t) \right] \\ &= n_{i,k} \cdot \exp [T \cdot \langle f_i(N_k) \rangle]. \end{aligned} \quad (4)$$

Here, $\langle f_i(N_k) \rangle$ is the average growth rate over the course of one period T at a given total population size N_k . We provide a formal derivation of this map in Appendix VII C. This approach has been used previously in Ref. [16] to derive certain mathematical properties of a class of models including Eq. (3), and it is similar to the averaging methods employed in Refs. [15, 32].

In the discrete map in Eq. (4), the externally imposed time dependence (the resource abundance $S(t)$ in the chemostat model) is integrated out. In other words, only the “time-averaged” effect of the explicitly time-dependent parameters is of relevance for this approximation. This greatly simplifies the qualitative analysis of the asymptotic dynamics of the population sizes at $t \rightarrow \infty$: for the continuous system, the population dynamics approach a limit cycle [Fig. 3c], but an analytic expression for the population sizes at the limit cycles can in general not be obtained due to the nonlinearity of the population dynamics. In the discrete map, however, the population dynamics approach a fixed point $\{n_j^*\}$ which can be calculated from Eq. (4). This allows to analyse the system quantitatively while preserving the qualitative features.

Figure 4 shows the time evolution in the form of a flow diagram for the population sizes $(n_{1,k}, n_{2,k})$ as obtained from the discrete map Eq. (4). Note that these flow diagrams do not show the population size variations over the course of a single period, but rather the change of the population sizes over subsequent periods $\{k, k+1, \dots\}$. Depending on the value of the activity ratio ν , qualitatively different dynamics are observed: In the absence of periodic changes of the environment ($\nu = 1$), the gleaner species n_1 is the surviving species, as indicated by the stable fixed point in the flow diagram (filled circle at $(n_{1,k}, n_{2,k}) = (\bar{N}_1, 0)$). This is the competitive exclusion principle. For a periodically changing environment with a sufficiently large activity ratio ($\nu > \nu_u$, [Fig. 4b]), the gleaner remains the surviving species. However, for a fine-tuned value of the activity ratio, $\nu = \nu_u$, the two non-trivial fixed points are stable simultaneously, as well as all states (n_1, n_2) along the heteroclinic orbit connecting these two fixed points. This corresponds to coexistence between the two species, where the final state of the system depends on the initial conditions. For activity ratios below this threshold ($\nu < \nu_u$, [Fig. 4d]), the opportunist is the surviving species. Thus, upon changing the activity ratio ν , the system exhibits a transition from competitive exclusion (gleaner survives) to inverse competitive exclusion (opportunist survives). In the following, we will quantify this transition and the threshold value ν for the activity ratio by generalizing the competitive exclusion principle to time-dependent environments.

2. Analogy to the competitive exclusion principle

Recall that in the autonomous system, the competitive exclusion principle states that the species with the smallest resource buffer or, equivalently, the largest maximally sustainable total population size $\bar{N}_i = S - \bar{K}_i$ will survive. If only one species prevails ($M = 1$), this largest sustainable total population size is identical to the steady-state population size n_i^* . In the non-autonomous system, the resource buffer \bar{K}_i is not well-defined due to the explicitly time-dependent growth rates f_i . However, it is possible to infer a proxy for the resource buffer from the steady-state population size in a single-species system: for the non-autonomous system, the analogue to each species’ steady-state population size is the population size at the fixed point of the discrete map in Eq. (4),

$$n_{i,k+1}(\{n_j^*\}) = n_{i,k}.$$

Following the line of arguments above in reverse, the fixed point in a system where only one species prevails ($M = 1$) corresponds to the largest sustainable population size, $\bar{N}_i = n_i^*|_{M=1}$. Equivalently, this allows to deduce a proxy resource buffer $S - n_i^*|_{M=1}$ for the time-dependent system. Based on this direct relation between the fixed point and the (proxy) resource buffer, we now generalize the competitive exclusion principle to systems with externally imposed time dependence (within in the

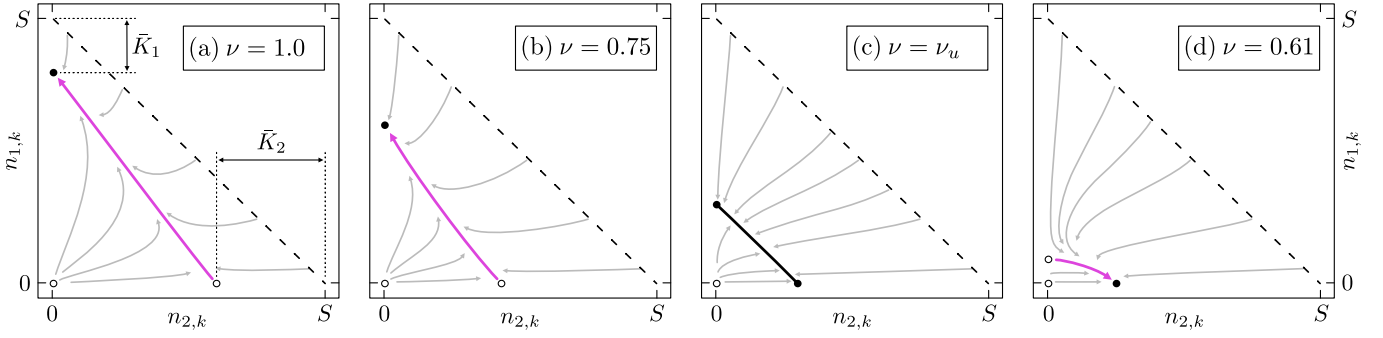


Figure 4. (Color online) Flow diagrams of the discretized population dynamics $(n_{1,k}, n_{2,k})$ obtained from the map Eq. (4) for the chemostat model at different values for ν as indicated in the graph; panel (c) shows the flow right at the upper activity ratio threshold $\nu_u \approx 0.64$. Pink (thick gray) lines represent heteroclinic orbits between the fixed points. At the threshold value ν_u for the activity ratio, all states on this orbit are stable (black line), corresponding to fine-tuned coexistence between the two species for a range of population size combinations (n_1, n_2) . For parameters see Table I.

range of validity of the discrete map): *In a system hosting two or more distinct species whose population dynamics are described by Eq. (3), competition will allow only one survivor, namely the one with the largest maximally sustainable total population size $\bar{N}_i \equiv n_i^*|_{M=1}$.*

The fixed point values – and thus also the maximally sustainable total population sizes \bar{N}_i – depend on the details of the external time dependence, which is effectively accounted for by the time-averaged growth rates $\langle f_i \rangle$ in the discrete map. In particular, they depend on the activity ratio, $\bar{N}_i(\nu)$, shown in Fig. 5a for two distinct species obeying the chemostat model. When these two species compete with each other, the one with the largest \bar{N}_i is predicted to survive. For all activity ratios above a threshold ν_u , the gleaner population n_1 is predicted to survive, since $\bar{N}_1 > \bar{N}_2$ in this parameter region, corresponding to the examples shown in Fig. 4b. In particular, the results from the autonomous system are recovered for $\nu = 1$, where $\bar{N}_i(1) = S - \bar{K}_i$ [Fig. 4a]. Right at the threshold, the maximally sustainable total population size is the same for both species, $\bar{N}_1(\nu_u) = \bar{N}_2(\nu_u)$, indicating fine-tuned coexistence between the two species [Fig. 4c]. Below the threshold, the opportunist species' maximally sustainable total population size is largest, $\bar{N}_1 < \bar{N}_2$, indicating that the opportunist survives [Fig. 4d]. The predicted survivor is indicated by the bars above the plot frame in Fig. 5a. So far, only the case $S' = 0$ (top row, solid lines) has been discussed; a generalization to $S' > 0$ will follow in Section III C.

3. Parameter regime for reversal of survival

Following the above generalisation of the competitive exclusion principle, the transition from regular to inverse competitive exclusion in a two-species system is found by determining the threshold value ν_u for which both species have the same maximally sustainable total population size, $\bar{N}_1(\nu_u) = \bar{N}_2(\nu_u)$. Graphically, ν_u can be

determined from the intersection of the functions $\bar{N}_i(\nu)$ [Fig. 5a]. Since the maximally sustainable total population size is derived from the single-species fixed points $n_i^*|_{M=1}$, one can use the discrete map in Eq. (4) to derive this threshold activity ratio. In particular, this requires to find the parameter combination (N, ν) at which both species' averaged growth rates are zero, i.e., solving the system of equations

$$0 = \langle f_1(\bar{N})|_{\nu_u} \rangle = \frac{1}{T} \int_0^T dt f_1(\bar{N}, t)|_{\nu_u} \quad (5a)$$

$$0 = \langle f_2(\bar{N})|_{\nu_u} \rangle \quad (5b)$$

for \bar{N} and ν_u . For the chemostat model with zero resources during the period of scarcity ($S' = 0$), this system of equations has only one physical solution, which we derive explicitly in Appendix VII D. Hence, in this case there is only one threshold activity ratio for which fine-tuned coexistence is possible [Fig. 5a], separating the regions of competitive exclusion and inverse competitive exclusion. The region of inverse competitive exclusion is bound from below by another threshold activity ratio ν_l , at which the overall resource abundance is too low to sustain the opportunist population. Thus, the externally imposed time dependence can lead to three distinct characteristic outcomes in the chemostat model with $S' = 0$: regular competitive exclusion, inverse competitive exclusion (enclosed by upper and lower boundaries ν_u and ν_l), and a system where neither species survives.

In general, there can be multiple threshold activity ratios (dashed lines in Fig. 5a for $S' > 0$), which can give rise to rich phase diagram structures. In any case, the region of inverse competitive exclusion extends only over a fraction of the entire parameter space, i.e., $0 < \nu_{u,l} < 1$ are strict bounds. This is evident since the cases $\nu = 1$ and $\nu = 0$ formally correspond to time-independent systems, for which regular competitive exclusion holds. Thus, if an upper boundary ν_u for the region of inverse competitive exclusion exists, then there is also a lower boundary ν_l ; however, the nature of this boundary can

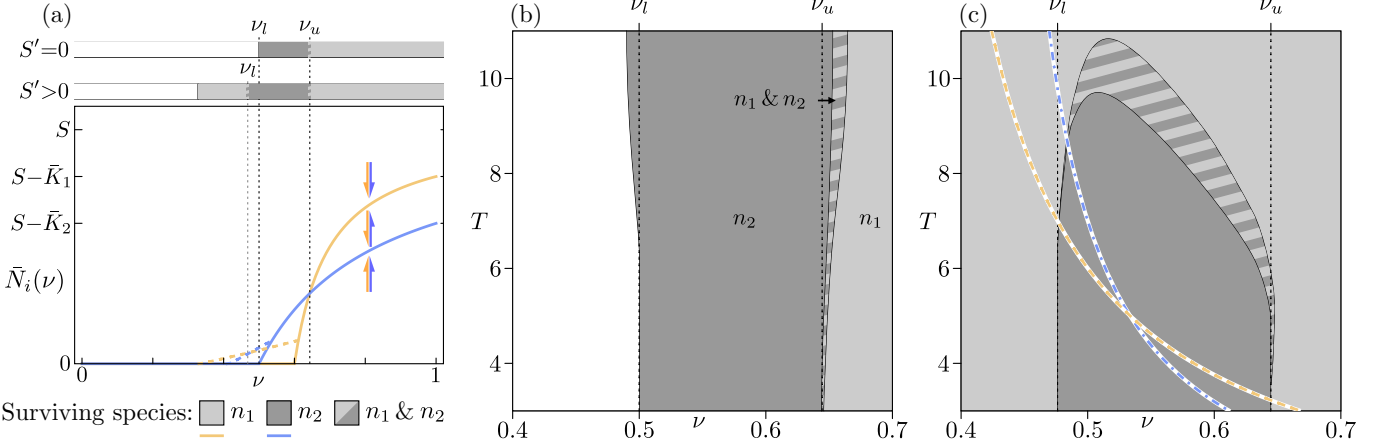


Figure 5. (Color online) Qualitative competition dynamics. (a) Maximally sustainable total population sizes $\bar{N}_i(\nu)$ as a function of the activity ratio ν (analogue to fixed points of the growth functions n_i^*) for two distinct species (gleaner shown in yellow or light gray, opportunist shown in blue or dark gray) that exhibit inverse competitive exclusion for time-dependent resource abundance in the chemostat model. Solid lines correspond to zero resources in times of scarcity ($S' = 0$), dashed lines show the fixed points for small but non-zero resources in this time window ($S' > 0$). Vertical dashed lines indicate the calculated upper and lower boundaries ν_u and ν_l to the region of inverse competitive exclusion. Arrows indicate the flow of the system towards the nullclines. Bars above indicate the surviving species over all values of the activity ratio ν for $T \rightarrow 0$ using $S' = 0$ and $S' > 0$, respectively. Shaded/patterned regions indicate which species survives. In this and all other figures showing bifurcation plots, uniformly shaded areas correspond to a single species surviving the competition, while striped areas correspond to coexistence between two species (c.f. legends below panel (a)). White areas indicate regions where neither species survives. (b) Representative bifurcation diagram for the chemostat model, which has no resources during episodes of scarcity ($S' = 0$). For short period durations T , the calculated phase boundaries ν_u and ν_l (dashed lines) agree well with the data (solid phase boundaries). Deviations at large T are due to nonlinearities in the population dynamics. (c) Representative bifurcation diagram for the chemostat model, which has small but finite resources during episodes of scarcity ($S' > 0$). Again, the calculated phase boundaries (black dashed lines) match the data (solid phase boundaries) at short T . As predicted by Eq. (23), no inverse competitive exclusion is possible at large T for any value of the activity ratio ν . At intermediate T , a band of coexistence connects the regions of regular and inverse competitive exclusion. For reference, the timescales of growth $\langle f_i(0, t) \rangle$ are shown for the gleaner (n_1 , yellow, dashed) and the opportunist (n_2 , blue, dash-dotted). For (b) and (c), the data was obtained as described in Appendix VII E, with simulated phase boundaries interpolated for better visual experience.

vary. Either, both species go extinct for $\nu < \nu_l$ (as in the case $S' = 0$ in the chemostat model), or there is another region of regular competitive exclusion (possible for $S' > 0$). We provide a detailed derivation of the threshold values $\nu_{u,l}$ in Appendix VII D.

The discrete map in Eq. (4) is based on the assumption that the period duration is much smaller than the time scales of growth, $T \ll f_i^{-1}$, and thus all ensuing predictions are expected to hold only in this parameter regime in general. In the chemostat model with $S' = 0$, however, numeric solutions of the system show that the predictions remain approximately valid for all period durations. A sample phase diagram for the two-species chemostat model is shown in Fig. 5b. The vertical dashed lines indicate the phase boundaries as predicted by the discrete map, which agree well with the numerically determined phase boundaries for short period durations. However, for large period durations, slight deviations from the predicted phase boundaries emerge: the region of inverse competitive exclusion (dark gray, labelled “ n_2 ”) broadens marginally. In addition, the fine-tuned coexistence at the upper boundary ν_u turns into a narrow band of coexistence (striped).

All significant deviations from the predicted phase boundaries happen within the parameter regime shown in Fig. 5b. In particular, the widths of the regions of inverse competitive exclusion and coexistence do not change anymore for even larger T . Note that the approximate validity of the predicted phase boundaries for all T is a special feature of the chemostat model. In essence, this is due to the fact that there is no competition during the period of scarcity if $S' = 0$ (without resources, there is no resource competition). As a consequence, the effects of the nonlinearities that were neglected in the discrete map are mostly suppressed for all T , resulting in only minimal changes to the phase diagram structure for large period durations. We provide a more formal explanation for this effect in Appendix VII D. In the following, we will turn towards a more general case and study the case where the nonlinearities are not suppressed.

C. Generalization to non-zero resources

So far, we have limited the analysis to ecosystems where no resources are available at all during the time

window when resources are scarce. Now, we relax this restriction and allow a limited amount but non-zero resources $0 < S' < S$. In this case, a finite amount of resources is always available, and therefore there is always resource competition between the two species. Thus, in contrast to the case $S' = 0$, the nonlinearities are now no longer suppressed. More precisely, nonlinear competition dominates the population dynamics once the total population size drops below the resource abundance, $N(t) < S(t)$. Since the gleaner population is less susceptible to resource scarcity and is less negatively affected by the competition than the opportunist, this implies that the gleaner gains an advantage during the period with absent resource. This effect counteracts the advantage that the opportunist gains from a quickly varying environment. Thus, inverse competitive exclusion as discussed above is not necessarily established if the total population size drops below the threshold value S' .

Under what conditions does the total population size drop below this threshold, $N(t) < S'$? This is the case only when the absolute duration of the periods with scarce resources is long compared to the time scales of growth, f_i^{-1} : for short period durations $T \ll f_i^{-1}$, the population sizes change only marginally during one cycle of the external oscillation, so that the total population size does not cross the threshold value S' . Consequently, the previously derived results (for $S' = 0$) and phase boundaries still apply in this more general case for $T \ll f_i^{-1}$: for a range of activity ratios ν , there is inverse competitive exclusion (dark gray region in Fig. 5c). In contrast, the population sizes change significantly for long period durations $T \gg f_i^{-1}$, so that the total population size can cross the threshold S' during the time window of scarce resources. As discussed above, this means that the gleaner species gains an advantage, so that regular competitive exclusion is restored in this parameter range.

Figure 5c shows an exemplary phase diagram for a two-species chemostat model with $S' > 0$. The predictions from the discrete map in Eq. (5) (in particular, the maximally sustainable total population sizes \bar{N}_i) for this specific system are shown in Fig. 5a as dashed lines. The phase diagram differs from the phase diagram corresponding to $S' = 0$ in three aspects. First, the lower phase boundary ν_l is shifted as a result of the nonlinear resource competition. Second, since the gleaner can now feed on the small amount of resources during the period of scarcity, it can survive for a range of activity ratios *smaller* than the lower phase boundary ν_l , instead of going extinct (light gray region). Third, the region of inverse competitive exclusion does not extend to $T \rightarrow \infty$, but is capped by a band of coexistence instead (striped). This band of coexistence is discussed in further detail in Appendix VII D. For reference, the time scales of growth f_i^{-1} are shown as dashed lines, indicating that the range of validity of the discrete map has an upper limit where the period durations are of the order of magnitude of the time scales of growth. It should be noted that the f_i^{-1}

themselves are only approximations of the actual time scales, as they neglect the nonlinear dynamics. Thus, different to the activity ratio thresholds, the time scales of growth should only be considered as qualitative estimates of the phase boundaries along the T -axis, and not as quantitative predictions.

Note that the type of coexistence encountered here is substantially different from the type of coexistence that arises when distinct species occupy temporal niches [3, 28, 34, 54]. Usually, “temporal niches” refers to a time-dependent system where the growth of different species is enhanced or inhibited in subsequent time windows [15, 55]. In the chemostat model, this could be the case for time-dependent per-capita growth rates $\mu_i(t)$, for example. In contrast, all species are treated equally in our setting. Here, coexistence originates from the nonlinear dynamics, meaning that the interactions between the populations are the cause of relative growth enhancement or inhibition. The temporal structure merely serves to keep the system at a conformation where the nonlinearities actually lead to coexistence. Hence, the time-dependent chemostat model at hand exhibits self-shaped niches, in contrast to externally imposed temporal niches.

IV. MANY-SPECIES COMPETITION

Until now, we explained how coexistence and inverse competitive exclusion can arise in a time-dependent environment hosting two species. However, natural ecosystems outside laboratory conditions typically consist of more than two species. In a time-independent environment, the competitive exclusion principle holds for an arbitrary number of species [43, 44]. In contrast, it is known that competitive exclusion can be overcome for resource competition in time-dependent environments, e.g. by successive temporal niches [3, 34], by introducing biotic resources [27, 35, 49], or both [28, 54]. However, it is not clear in general how multiple competing species with complex interaction networks can coexist in a temporally varying environment. In the following, we demonstrate how the qualitative dynamics of such complex networks can be assessed by means of the theoretical framework that we used to analyze the two-species competition in Section III.

In order to understand the population dynamics of M competing species (M -species competition), it is important to realize that the knowledge about pairwise interactions between a set of species can – to some extent – provide information about the overall community interactions [45, 46, 56]. In fact, for a biological system where only the total population size is relevant for the competition, it is sufficient to consider pairwise interactions only; the validity of this statement is shown in Appendix VII F. Heuristically, this follows from the fact that the relative impact of a species on the competition decreases as its relative population size, n_i/N , decreases. Consequently, the species with the largest population size has dominant

impact on the competition, and thus can be regarded as the main competitor for all other species. Combining the insights from all pairwise interactions, this allows to characterize the phase diagram for many-species competition. In the following we explicitly demonstrate this for three-species competition.

A. Bifurcation diagram

Consider an ecosystem hosting three different species, each obeying Eq. (2). The species are ranked from smallest to largest resource buffer in the following, so that $\bar{K}_1 < \bar{K}_2 < \bar{K}_3$ (full parameter set in Table I). With constant resource abundance only the species with the lowest resource buffer can survive as consequence of competitive exclusion (n_1 with the specified ranking). The two other species will go extinct successively: first, the species with the largest resource buffer (n_3), and afterwards the species with moderate resource buffer (n_2). In terms of pairwise interaction, the moderate species n_2 takes the role of the opportunist when competing with n_1 , and it takes the role of the gleaner when competing with n_3 . For all pairwise interactions, the species with highest (lowest) resource buffer always takes the role of the opportunist (gleaner).

When the resource abundance switches periodically, the relative competitive advantages between pairs of species can be altered, in accordance with the observations in Section III: for each pair of species, there may exist a range of activity ratios ν and period durations T for which regular competitive exclusion does not take effect, and instead the pair shows inverse competitive exclusion or coexistence [Fig. 5]. In the three-species chemostat model with equal washout rates δ , coexistence between all three species due to the time-dependent environment can be achieved when at least two out of the three pairs of species establish pairwise coexistence.

The most suitable representation for M -species competition is a phase diagram, which can be inferred from the set of all two-species phase diagrams. The two-species diagrams for the sample system specified in Table I are shown in Figs. 6a-c, which were each obtained by eliminating one of the three species from the system and then solving the corresponding ODEs numerically. The characteristics of these phase diagrams can be calculated analytically as shown in Section III. Notably, each of the three subsystems shows regions of inverse competitive exclusion and coexistence. The phase diagram for three-species coexistence is shown in Fig. 6d overlaid with the phase boundaries from all pairwise competitions.

The phase boundaries from pairwise competition predominantly match the three-species diagram, owed to the fact that pairwise competition is sufficient to explain M -species competition. For the specific system shown in Fig. 6, the population n_3 outcompetes the other two populations individually in the parameter range $0.8 \lesssim T \lesssim 1.0$ and $0.25 \lesssim \nu \lesssim 0.45$ (dark gray regions in

Fig. 6c, which is also enclosed by the dark gray region in Fig. 6b). In this parameter range, the population n_2 outcompetes n_1 (medium gray region in Fig. 6a). Therefore, in three-species competition, the population n_1 is outcompeted jointly by n_2 and n_3 , and subsequently the latter outcompetes the former, so that only n_3 survives in the specified parameter regime (dark gray region in Fig. 6d). Similarly, the overall gleaner n_1 is defeated by n_2 and n_3 independently in pairwise competition across the entire parameter range for which coexistence between n_2 and n_3 is possible (striped region in Fig. 6c). Thus, in three-species competition, the overall gleaner n_1 cannot survive in this parameter region either. Consequently, the phase boundaries from pairwise competition between n_2 and n_3 are valid for the three-species competition in this parameter region, too (same region in Fig. 6d). These rules for inferring the surviving species in M -species competition apply for the almost the entire parameter space, with exceptions where regions of pairwise coexistence overlap (see below). To demonstrate this for the specific example shown here, the phase boundaries from pairwise competition [Fig. 6a-c] are indicated as white lines in Fig. 6d.

B. Three-species coexistence

Deviations from the two-species phase boundaries occur where nonlinearity dominates the population dynamics. In particular, there is a transient region of three-species coexistence in the overlap region of pairwise coexistence between n_1 and n_2 , and n_1 and n_3 , respectively (black region in Fig. 6d). Qualitatively, this transient region can be understood from pairwise competition, too: at the onset of pairwise n_1 - n_2 -coexistence (diamond symbol in Fig. 6d), close to the region of inverse competitive exclusion, the dominant species is n_2 [Fig. 6g]. In the same parameter region the overall gleaner n_3 goes extinct in n_2 - n_3 -competition, meaning that also here n_2 is the dominant species. Thus, for three-species competition, there is n_1 - n_2 -coexistence as long as n_2 remains the dominant species in pairwise interactions.

Upon increasing the period duration T , approaching the triangle symbol in Fig. 6d, n_1 takes over as the dominant species in pairwise coexistence with n_2 . n_1 can coexist with both n_2 and n_3 in this parameter region [Fig. 6f]. Thus, a band of three-species coexistence emerges at this intermediate T . Finally, upon further increasing the period duration T , n_2 and successively n_3 go extinct in pairwise competition with n_1 . In three-species competition, this corresponds to a region of n_1 - n_3 -coexistence, followed by regular competitive exclusion.

In the preceding discussions, we restricted the analysis to populations with identical decay rates δ . This fixes a global time scale for the population dynamics of all species. However, these rates can be different when the decay is not dominated by uniform washout from a chemostat. In this case, the time scales of the growth

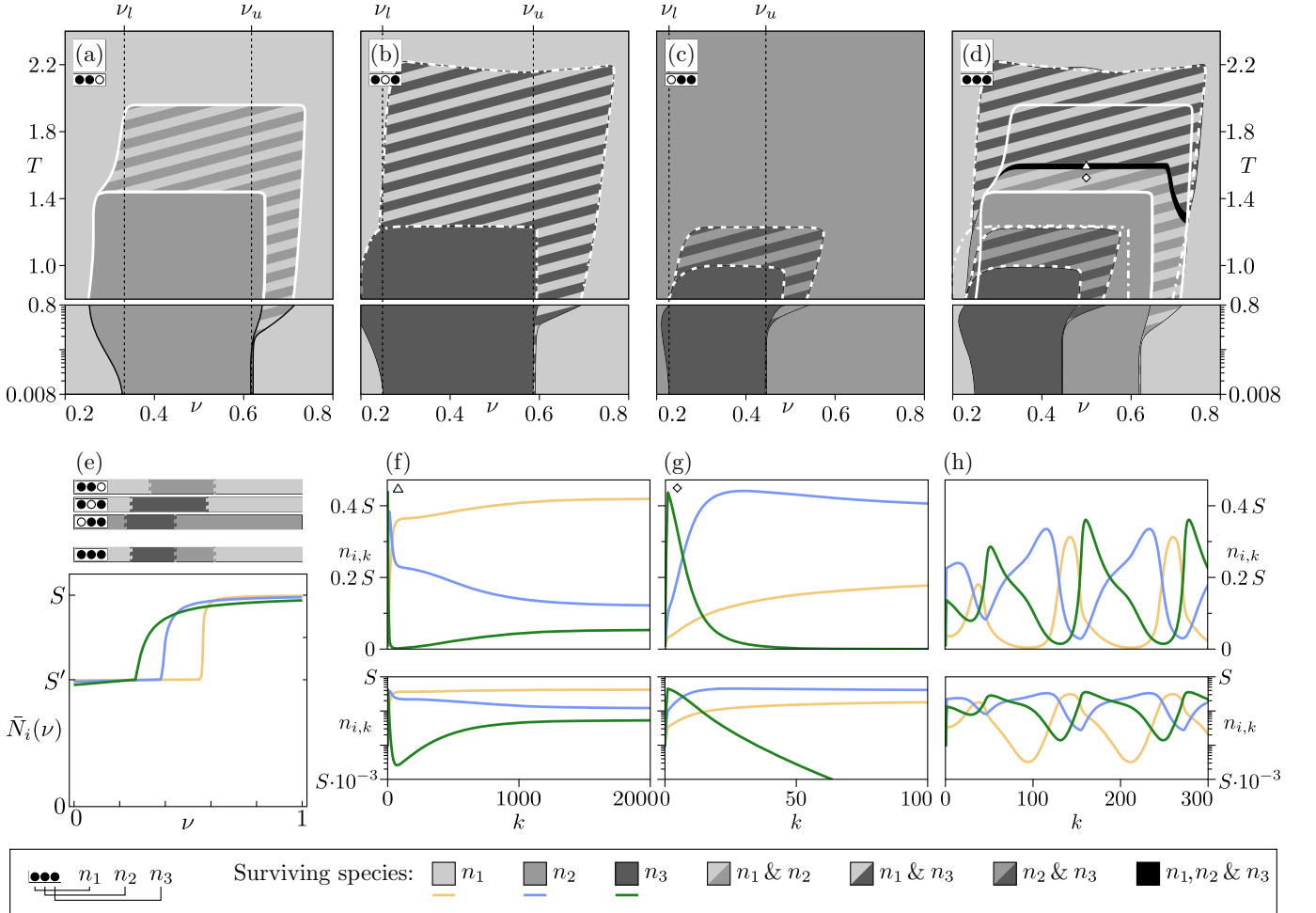


Figure 6. (Color online) Three-species competition. For each bifurcation diagram, filled (open) circles indicate that the corresponding species takes part (does not take part) in the competition. (a-c) Phase diagrams for pairwise competition with parameters as specified in Table I. White lines indicate phase boundaries for reference in panel (d). For the chosen parameter set, each pair of species exhibits a region of inverse competitive exclusion and coexistence. The (vertical) dashed black lines indicate the calculated phase boundaries for the limit $T \rightarrow 0$. (d) Phase diagram for the competition of all three species. The two-species phase boundaries (white lines) are copied from the pairwise phase diagrams and show good agreement with the actual phase boundaries for the three-species system. The phases for three-species competition can be predicted from combining the pairwise phase diagrams. (e) Fixed points of the growth functions for the species shown in (a-d), exhibiting overlapping parameter ranges for the activity ratio ν with inverse competitive exclusion. Bars above the fixed points indicate the surviving species as predicted by the linearized map for $T \rightarrow 0$. (f, g) Sample trajectories for three-species competition, with coexistence between all three species (f) and pairwise n_1 - n_2 -coexistence (g), on a linear scale (top) and log scale (bottom) for better visibility. The corresponding values of ν and T for these trajectories are marked in the three-species bifurcation diagram as triangle (f) and diamond (g). (h) Sample trajectory of three-species competition with $\delta_i \neq \delta_j$, showing limit cycle dynamics instead of approaching a fixed point. The corresponding parameters are specified in Table I.

dynamics can be different for each species. This leads to a more complex dependence of the pairwise coexistence regions on the period duration T and can result in additional types of coexistence. For example, Fig. 6h shows a system where the time-dependent environment leads to pairwise coexistence between the overall gleaner and the overall opportunist, but leaves all other pairwise interactions untouched. In the corresponding three-species ecosystem, the population sizes after k periods, $n_{i,k}$, slowly vary in a Lotka-Volterra-like fashion in ad-

dition to the oscillating dynamics, $n_i(t)$, over the course of a single period T of the external time dependence. This suggests that such a time-dependent population dynamics system could be reduced to a time-independent Lotka-Volterra system, whose dynamics have been studied exhaustively, allowing for a more abstract description of time-dependent environments [57]. A thorough analysis of this phenomenon is yet to be done.

V. DISCUSSION AND CONCLUSION

In summary, we analyzed how coexistence between multiple species can be achieved in an explicitly time-dependent variant of the chemostat model. We showed that the principle of competitive exclusion, which holds for time-independent models, does not necessarily apply anymore in the time-dependent variant. Instead, the ecosystem can be deterred from reaching a steady state at which competitive exclusion applies, thus giving rise to interesting and rich population dynamics.

Our analysis of the population dynamics in a two-species chemostat system with temporally varying resource abundance shows that the competitive exclusion principle can be generalized to time-dependent systems by calculating a steady-state population size from an approximate discretized map. Importantly, we demonstrate that this map is sufficient to understand the qualitative population dynamics in a general time-dependent system. In particular, we inferred from this analysis that there can be coexistence between two species when the population dynamics are in ‘resonance’ with the time-dependent environment.

Generalizing to systems with three species, we demonstrated how complex population profiles in three-species systems can be deduced qualitatively from pairwise interactions. One of our key findings here was that a time-dependent environment can allow three-species coexistence, even if – as a consequence of competitive exclusion – only one species can survive in a time-independent environment.

Notably, this kind of qualitative analysis, where pairwise interactions are used to infer the population dynamics of the full system, can be extended to many-species systems. As the number of species increases, an analytic study of the ODEs describing the population dynamics of the full system becomes increasingly difficult. In contrast, pairwise competition can be assessed analytically, accurately predicting regimes of inverse competitive exclusion. This is in line with results from recent experimental work on *in vitro* ecosystems [46] and the *C. elegans* intestinal microbiome [58], where the composition of the full ecosystem can be inferred from the composition of a set of subsystems. Due to the nonlinearity of the ODEs – typically originating from saturation effects of the limiting resource in population dynamics models – the analysis of pairwise coexistence remains on a qualitative level, and further work will be required to elucidate

this particularly interesting regime. In general, however, insights from a pairwise analysis can be combined to predict the qualitative outcome of the many-species system.

In this article, we limited our discussions to competing species models, with examples focused on chemostat systems. In these systems, the interactions between the species often depend exclusively on the total population size. In realistic ecosystems, however, populations can interact via many different mechanisms, such as sharing of multiple resources [34], the production of a common good [59–62], or the production of a toxin [63, 64]. In addition, populations in realistic ecosystem can be spatially structured, such that competition between species happens only at the boundaries of single-species communities [65, 66]. Our results suggest that a time-dependent environment may be capable of enhancing the biodiversity in these systems, similar to the competing species model. However, a comprehensive analysis of the population dynamics in these systems in the presence of a time-dependent environment is still lacking. Further extensions of the model discussed here could include the effect of demographic noise on the population dynamics, which is likely to play a decisive role in the highly nonlinear coexistence regime [37, 39].

On a more general level, our results demonstrate the role of a time-dependent environment on the composition of an ecosystem. In particular, our findings show that biodiversity can be enhanced by such a temporally varying environment. In other words, ecosystems with high biodiversity may lose this diversity when removing an external fluctuation from the system. This suggests that realistic ecosystems may depend crucially on natural environmental cycles, such as the circadian sunlight cycle or tidal ranges. To test this hypothesis, experimental studies of ecosystems subject to temporal variations will be needed.

VI. ACKNOWLEDGEMENTS

We thank M. Merrow and Z. Chen for stimulating discussions and valuable input, and F. Raßhofer for critical reading of the manuscript. We acknowledge financial support by the Deutsche Forschungsgemeinschaft through the Excellence Cluster ORIGINS under Germany’s Excellence Strategy (EXC-2094-390783311), and the funding initiative “What is life?” of the VolkswagenStiftung.

[1] D. J. Schaeffer, E. E. Herricks, and H. W. Kerster, Environmental Management **12**, 445 (1988).

[2] D. J. Rapport, R. Costanza, and A. J. McMichael, Trends in Ecology & Evolution **13**, 397 (1998).

[3] P. Chesson, Annual Review of Ecology and Systematics **31**, 343–366 (2000).

[4] S. T. Jackson and D. F. Sax, Trends in Ecology & Evolution , 1 (2009).

[5] A. T. Reese and R. R. Dunn, mBio **9**, 734 (2018).

[6] M. H. Zwietering, I. Jonenburger, F. M. Rombouts, and K. van’t Riet, Applied and Environmental Microbiology **56**, 1875 (1990).

[7] J. Monod, Annual Review of Microbiology **3**, 371 (1949).

[8] E. Litchman and C. A. Klausmeier, *The American Naturalist* **157**, 170 (2001).

[9] D. A. Ewing, C. A. Cobbold, B. V. Purse, M. A. Nunn, and S. M. White, *Journal of Theoretical Biology* **400**, 65 (2016).

[10] X. Liang and G. A. FitzGerald, *Journal of biological rhythms* **32**, 505 (2017).

[11] P. Burt, S. Grabe, C. Madeti, A. Upadhyay, M. Merrow, T. Roenneberg, H. Herz, and C. Schmal, *iScience* **24**, 103370 (2021).

[12] P. Ma, T. Mori, C. Zhao, T. Thiel, and C. H. Johnson, *PLoS Genetics* **12**, e1005922 (2016).

[13] C. Thaiss, D. Zeevi, M. Levy, G. Zilberman-Schapira, J. Suez, A. Tengeler, L. Abramson, M. Katz, T. Korem, N. Zmora, Y. Kuperman, I. Biton, S. Gilad, A. Harmelin, H. Shapiro, Z. Halpern, E. Segal, and E. Elinav, *Cell* **159**, 514 (2014).

[14] A. Zarrinpar, A. Chaix, S. Yooseph, and S. Panda, *Cell Metabolism* **20**, 1006 (2014).

[15] J. M. Cushing, *Theoretical Population Biology* **30**, 289 (1986).

[16] R. R. Vance, *Theoretical Population Biology* **37**, 438 (1990).

[17] J. Baranyi, T. A. Roberts, and P. McClure, *Food Microbiology* **10**, 43 (1993).

[18] J. Baranyi, T. A. Roberts, and P. McClure, *Mathematical Medicine and Biology A Journal of the IMA* **10**, 293 (1993).

[19] R. R. Vance and E. A. Coddington, *Journal of Mathematical Biology* **27**, 491 (1989).

[20] B. D. Coleman, Y.-H. Hsieh, and G. P. Knowles, *Mathematical Biosciences* **46**, 71 (1979).

[21] B. D. Coleman, *Mathematical Biosciences* **45**, 159 (1979).

[22] T. G. Hallam and C. E. Clark, *Journal of Theoretical Biology* **93**, 303 (1981).

[23] S. S. Pilyugin and P. Waltman, *Mathematical Biosciences* **182**, 151 (2003).

[24] S. Rosenblat, *Journal of Mathematical Biology* **9**, 23 (1980).

[25] R. M. Nisbet and W. S. C. Gurney, *Journal of Theoretical Biology* **56**, 459 (1976).

[26] J. M. Cushing, *Journal of Mathematical Biology* **10**, 385 (1980).

[27] M. C. White and X.-Q. Zhao, *Bulletin of Mathematical Biology* **71**, 145 (2008).

[28] R. Levins, *The American Naturalist* **114**, 765 (1979).

[29] J. K. Hale and A. S. Somolinos, *Journal of Mathematical Biology* **18**, 255 (1983).

[30] T. Namba, *Journal of Theoretical Biology* **111**, 369 (1984).

[31] S. B. Hsu, *Journal of Mathematical Biology* **9**, 115 (1980).

[32] P. de Mottoni and A. Schiaffino, *Journal of Mathematical Biology* **11**, 319 (1981).

[33] M. C. Gallagher, M. Arnold, E. Kadaub, S. Culloty, R. M. O’Riordan, R. McAllen, and D. Rachinskii, *Theoretical Population Biology* **131**, 12–24 (2020).

[34] R. A. Armstrong and R. McGehee, *Theoretical Population Biology* **9**, 317–328 (1976).

[35] A. L. Koch, *Journal of Theoretical Biology* **44**, 373–386 (1974).

[36] S. Maslov and K. Sneppen, *Scientific reports* **7**, 1 (2017).

[37] K. Wienand, E. Frey, and M. Mobilia, *Phys. Rev. Lett.* **119**, 158301 (2017).

[38] K. Wienand, E. Frey, and M. Mobilia, *Journal of The Royal Society Interface* **15**, 20180343 (2018).

[39] A. Taitelbaum, R. West, M. Assaf, and M. Mobilia, *Phys. Rev. Lett.* **125**, 048105 (2020).

[40] J. Pande and N. M. Shnerb, *Population dynamics in stochastic environments* (2020), arXiv:2007.10048 [q-bio.PE].

[41] Y. Yahalom, B. Steinmetz, and N. M. Shnerb, *Phys. Rev. E* **99**, 062417 (2019).

[42] P. G. Hufton, Y. T. Lin, and T. Galla, *Phys. Rev. E* **99**, 032122 (2019).

[43] R. A. Armstrong and R. McGehee, *The American Naturalist* **115**, 151–170 (1980).

[44] G. Hardin, *Science* **131**, 1292 (1960).

[45] K. Faust and J. Raes, *Nature Reviews Microbiology* **10**, 538 (2012).

[46] J. Friedman, L. M. Higgins, and J. Gore, *Nature Ecology & Evolution* **1**, 1 (2017).

[47] J. P. Grover, *Resource Competition*, Vol. 19 (Springer US, Boston, MA, 1997).

[48] H. L. Smith and P. Waltman, *The Theory of the Chemostat* (Cambridge University Press, 1995) p. 313.

[49] D. Tilman, *Resource competition and community structure* (Princeton University Press, 1982) p. 296.

[50] E. T. Miller and C. A. Klausmeier, *Theoretical Ecology* **Theoretical Ecology**, 91–103 (2017).

[51] A. Burson, M. Stomp, E. Greenwell, J. Grosse, and J. Huisman, *Ecology Ecology*, **99**, 1108–1118 (2018).

[52] H. L. Smith, *Journal of Differential Equations* **64**, 165–194 (1986).

[53] M. W. Hirsch, *SIAM Journal on Mathematical Analysis* *SIAM Journal on Mathematical Analysis*, **13**, 167–179 (1982).

[54] S. Nowack and I. Klapper, *SIAM Journal on Applied Mathematics* **78**, 2819–2839 (2018).

[55] J. Tan, C. K. Kelly, and L. Jiang, *Nature communications* **4**, 1 (2013).

[56] C. A. Klausmeier, *Journal of Theoretical Biology* **262**, 584 (2010).

[57] J. Hofbauer and K. Sigmund, *Evolutionary games and population dynamics* (Cambridge University Press, Cambridge, 1998).

[58] A. Ortiz, N. M. Vega, C. Ratzke, and J. Gore, *The ISME Journal* **15**, 2131 (2021).

[59] S. A. West, A. S. Griffin, A. Gardner, and S. P. Diggle, *Nature reviews microbiology* **4**, 597 (2006).

[60] J. S. Chuang, O. Rivoire, and S. Leibler, *Science* **323**, 272 (2009).

[61] F. Becker, K. Wienand, M. Lechner, E. Frey, and H. Jung, *Scientific Reports* **8**, 4093 (2018).

[62] J. Cremer, A. Melbinger, K. Wienand, T. Henriquez, H. Jung, and E. Frey, *Journal of Molecular Biology* **431**, 4599 (2019).

[63] T. L. Czárán, R. F. Hoekstra, and L. Pagie, *Proceedings of the National Academy of Sciences* **99**, 786 (2002).

[64] M. F. Weber, G. Poxleitner, E. Hebsch, E. Frey, and M. Opitz, *Journal of the Royal Society Interface* **11**, 20140172 (2014), 1405.5025.

[65] T. Reichenbach, M. Mobilia, and E. Frey, *Nature* **448**, 1046 (2007).

[66] U. Dobramysl, M. Mobilia, M. Pleimling, and U. C. Täuber, *Journal of Physics A: Mathematical and Theoretical* **51**, 063001 (2018).

VII. APPENDIX

A. Resource Buffer \bar{K}_i

The population dynamics of competing species as described in the main matter follows the chemostat model

$$\frac{dn_i(t)}{dt} = n_i(t) \cdot \left(\mu_i \frac{S - N(t)}{S - N(t) + K_i} - \delta_i \right). \quad (6)$$

Consider a system inhabited by a single species, so that $N(t) = n_i(t)$. The differential equation 6 has two fixed points, $n_i(t) = 0$ and $n_i(t) = S - \bar{K}_i =: \bar{N}_i$, with \bar{K}_i given by

$$\bar{K}_i = \frac{\delta_i}{\mu_i - \delta_i} K_i. \quad (7)$$

This offset denotes the amount of resources that are left unbond by the species i upon reaching its non-zero steady state. This is a direct effect of the resource-limited Monod-like growth. In a system hosting two species, the resources left unbound by species i are available for species j . However, species j can only feed on them if its own resource buffer \bar{K}_j is not reached yet, i.e. if $\bar{K}_j < \bar{K}_i$. This is the competitive exclusion principle.

If the time dependence does not affect the amount of resources, but any of the other system parameters, then the resource buffer may become time-dependent itself,

$$\bar{K}_i(t) = \bar{K}_i(\mu_i(t), \delta_i(t), K_i(t)). \quad (8)$$

Similar to the case of time-dependent resources abundance, this may lead to coexistence and inversion, but also allows for temporal niches [3, 28, 34, 54].

B. Constraints on the growth function f_i

In the general growth model class of competing species models, the population dynamics are governed by a growth function $f_i(N(t), t)$ [53]:

$$\frac{dn_i(t)}{dt} = n_i(t) \cdot f_i(N(t), t). \quad (9)$$

Between two species, the growth functions f_i can in general differ at certain parameters (e.g., different growth rates μ_i), or the f_i may be completely different functions of the parameters. For a growth function to be realistic and biologically meaningful, it needs to meet several requirements: (i) The concept of *competing* species is incorporated in this function by requiring that – for any species – the growth should be slower if any population size increases (while all others remain constant). (ii) In an almost abandoned environment ($N \rightarrow 0$), growth should always be possible. (iii) There should be a single threshold population size n_i^* at which the population cannot grow anymore, and above which the growth is

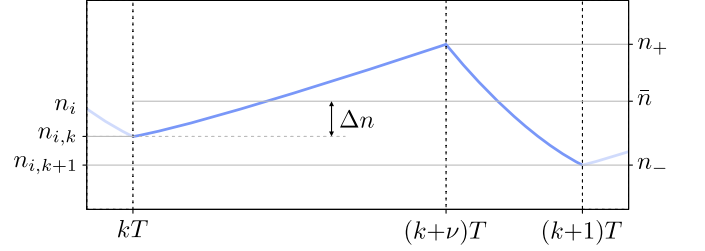


Figure 7. (Color online) Conceptual time evolution of the population size of a single species over one period. For the entire period, the population size remains within an interval bounded by n_+ and n_- . Note that in the chemostat model as defined in Eq. (6), the minimal population size n_- coincides with $n_{i,k+1}$, which need not be the case in general.

negative, as the system can only sustain a limited number of individuals. Mathematically, the conditions (i)-(iii) can be expressed as

$$(i) \quad \frac{\partial}{\partial n_j} f_i(N(t), t) < 0, \quad (10a)$$

$$(ii) \quad f_i(N \rightarrow 0, t) > 0, \quad (10b)$$

$$(iii) \quad f_i(N > \bar{N}_i, t) < 0. \quad (10c)$$

In addition, to ensure continuous dynamics, the growth functions f_i need be finite for all states that are accessible in reality, i.e. for all $\{n_j > 0\}$.

C. Derivation of the discrete map

In competing species models, the population dynamics are determined by the growth functions f_i . The functional form of the growth functions is determined by the system under investigation. The wide variety of ecosystems and models makes it difficult to make general statements about the population dynamics, or let alone solve the corresponding differential equations analytically. In addition, a common feature of most population dynamics models, and in particular of the competing species models, is the nonlinearity of the differential equations that represent the population dynamics, which further complicates the analysis. However, the nonlinearity can be neglected to lowest order when propagating the system over short time intervals for any competing species model, as we will show in the following.

Consider a system hosting one species only. To further simplify the explanations, we begin by defining two new quantities: over the course of one oscillation, the population size will reach a local maximum n_+ and a local minimum n_- [Fig. 7]. We will demonstrate in the following that the error introduced by the approximate map is to lowest order proportional to T/f_i^{-1} within a single period. To see this, formally solve the differential equation 3a for a single species, i.e., for the case where

$$N(t) = n_i(t):$$

$$n_i(t+T) = n_i(t) \cdot \exp \left[\int_t^{t+T} du f_i(n_i(u), u) \right]. \quad (11)$$

Making use of the competition condition in Eq. (3b), stating that $\partial_{n_i} f_i \leq 0$, it follows that the growth function in the integral is bounded from above and below by n_+ and n_- . In addition, for any arbitrary external time dependence, there is always one u_+ (u_-) that maximizes (minimizes) the growth function at a constant population size, so that

$$f_i(n_-, u_-) < f_i(n_i(u), u) < f_i(n_+, u_+) \quad \forall u \in [t, t+T]. \quad (12)$$

This allows to calculate upper and lower bounds to the integral in Eq. (11), and thus also for the population size after one period:

$$n_- e^{f_i(n_-, u_-)T} < n_i(t+T) < n_+ e^{f_i(n_+, u_+)T}. \quad (13)$$

Expanding the exponential to lowest order in T , this shows that the population varies within a range proportional to T over a single period. In addition, from the mean value theorem it follows that there exists a constant \bar{n} with $n_- < \bar{n} < n_+$ [Fig. 7] so that

$$n_i(t+T) = \bar{n} \cdot \exp \left[\int_t^{t+T} du f_i(\bar{n}, u) \right]. \quad (14)$$

This \bar{n} differs from the population size at the beginning of the period $n_{i,k}$ by $\bar{n} = n_{i,k} + \Delta n$. Notably, from the definition of \bar{n} it follows immediately that $\Delta n < n_+ - n_- \sim \mathcal{O}(T/f_i^{-1})$. Thus, expanding the growth function around \bar{n} , we find

$$f_i(n_{i,k}, u) = f_i(\bar{n}, u) + \partial_{n_i} f_i(\bar{n}, u) \Delta n + \mathcal{O}(\Delta n^2). \quad (15)$$

Substituting this into Eq. (14) and renaming $n_i(t+T)$ to $n_{i,k+1}$ leads – to lowest order in T/f_i^{-1} – to the discrete map from Eq. (4):

$$\begin{aligned} n_{i,k+1} &= n_{i,k} \cdot \exp \left[\int_t^{t+T} du f_i(n_{i,k}, u) \right] + \mathcal{O}(\Delta n) \\ &= n_{i,k} \cdot \exp \left[\int_t^{t+T} du f_i(n_{i,k}, u) \right] + \mathcal{O}(T/f_i^{-1}). \end{aligned} \quad (16)$$

The same argument holds for a system hosting more than one species. In this case, the upper and lower limits n_{\pm} as well as the constant \bar{n} are replaced by a set of corresponding quantities. The decisive observation, namely that $\Delta n_i < n_{i,+} - n_{i,-} \sim \mathcal{O}(T/f_i^{-1})$, remains valid for any number of species. Thus, the discrete map Eq. (4) approximates the exact dynamics up to $\mathcal{O}(T/f_i^{-1})$, making it reasonable for period durations short compared to the time scales of growth.

D. Derivation of phase boundaries

In a nonlinear competing species model hosting two species, the time-dependent environment can lead to an inversion of the competitive exclusion principle, and possibly coexistence. Such inversion and coexistence can only be established for a range of parameters. For two given species in an environment that switches between two given distinct states, the parameters that quantify the temporal structure are the duration of one period T and the fraction of one period ν that is spent in one of the two states. Note that for other time-dependent systems, for example an environment that changes continuously, there may be other parameters that quantify the temporal structure. In the following, we will explain how the phase boundaries to inverse competitive exclusion and to coexistence can be obtained for a general system of two competing species. Along the lines, we will discuss in detail how the phase boundaries on ν and T are obtained for the chemostat model with varying resources. Throughout this discussion, the species are labeled such that n_1 is the gleaner and n_2 is the opportunist ($\bar{K}_1 < \bar{K}_2$).

1. Formal derivation

For the purpose of determining the biodiversity of an ecosystem, we distinguish between four distinct states of the system: (i) the gleaner survives, (ii) the opportunist survives, (iii) both populations survive, or (iv) neither population survives. In a time-independent environment, the asymptotic state of the system can be obtained by performing a linear stability analysis on the fixed points n_i^* of the ODEs modeling the population dynamics. However, this is not possible in a time-dependent environment, since the fluctuation of model parameters prevents the system from reaching a steady state. Thus, the asymptotic dynamics of such a system are periodic trajectories, $n_i^*(t)$, rather than fixed points. In a nonlinear system, these trajectories can in general only be determined exactly by numerically solving the ODEs, which yields little information about the conceptual dynamics. By approximating the asymptotic trajectories, however, the phase boundaries can be estimated.

In a two-species system, the two asymptotic trajectories where only one of the two populations, n_i , survives while the other is extinct, respectively, are of particular relevance. Formally, the stability of these asymptotic trajectories with respect to invasion by the other species n_j can be assessed from the average net growth rate

$$\langle f_j \rangle(t) = \frac{1}{T} \int_t^{t+T} du f_j(\{n_i^*(u)\}, u), \quad (17)$$

where $n_i^*(u) \approx N(t)$ is the asymptotic trajectory of the prevailing species and $n_j(u) \approx 0$ is negligibly small. By comparing this to Eq. (11), it is obvious that $n_{j,k+1} =$

$n_{j,k} \exp[T \cdot \langle f_j(kT) \rangle]$. Thus, if the average net growth rate is positive (negative), the invading population grows (goes extinct) and the asymptotic trajectory of the prevailing species is unstable (stable). Hence, phase boundaries are located at parameter combinations where any average net growth rate changes sign.

2. Phase boundary on Inversion

To derive the phase boundaries to the region of inverse competitive exclusion, consider a system with a short period duration T compared to the time scales of growth, f_i^{-1} . As discussed in Appendix VII C, one may accurately approximate the exact population dynamics in the limit $T \ll f_i^{-1}$ by a discrete map

$$n_{i,k+1} = n_{i,k} \cdot \exp \left[\int_0^T dt f_i(N_k, t) \right]. \quad (18)$$

In particular, this map can be used to test whether one population can invade the other population. Inverse competitive exclusion means that the opportunist species n_2 can invade a residing gleaner population n_1 . In the following, we denote the steady state population size of the gleaner as n_1^* , such that $n_{1,k} = n_1^*$ for all k at the steady state. By definition, this steady state corresponds to the maximally sustainable total population size \bar{N}_1 . The opportunist can invade the gleaner population if the average net growth within one period is positive,

$$\langle f_2 \rangle(\nu) \Big|_{N=n_1^*} := \frac{1}{T} \int_0^T dt f_2(n_1^*, t) > 0. \quad (19)$$

Otherwise, the opportunist population will go extinct. By definition, this net growth is negative for time-independent environments, $\nu = 0$ and $\nu = 1$, and varies continuously when changing the activity ratio ν . Thus, if the net growth is positive for any value of ν , this implies that there are two threshold values for the activity ratio, ν_u and ν_l , at which $\langle f_2 \rangle(\nu_{u,l}) = 0$. These threshold values mark the phase boundaries of the region of inverse competitive exclusion at short period durations (Fig. 8).

Notably, the gleaner steady state population size depends on the activity ratio, too, $n_1^*(\nu)$, and hence also $\bar{N}_1(\nu)$. In particular, the gleaner species may not be able to survive even without competition for some activity ratios, such that $n_1^* = 0$. This is the case, for example, in the chemostat model (Eq. (2a)) for the lower boundary on the inversion region. For arbitrary ν , the discrete map can be used to formally obtain the gleaner steady state population size at $S' = 0$ for $T \ll f_i^{-1}$:

$$0 = \int_t^{t+T} du f_1(n_1^*(\nu), u),$$

$$\rightarrow n_1^*(\nu) \equiv \bar{N}_1(\nu) = S - K_1 \frac{\delta_1}{\mu_1 \nu - \delta_1}. \quad (20)$$

However, as only non-negative steady state population sizes are meaningful, this steady state population size will be zero when

$$\nu < \frac{\delta_1}{\mu_1} \cdot \frac{K_1 + S}{S} =: \nu_1.$$

A similar equation can be derived for the steady state population size of the opportunist. Thus, the opportunist can survive in an environment in which the gleaner goes extinct for $\nu_1 < \nu < \nu_2$. In particular, the smallest activity ratio for which the average net growth for the opportunist is positive is ν_2 , so that the lower bound to the region of inverse competitive exclusion is $\nu_l = \nu_2$ [Fig. 5a].

The upper bound to the phase of inverse competitive exclusion in the chemostat model can be calculated straightforwardly by solving $\langle f_2 \rangle(\nu_u) = 0$ using the expression for $n_1^*(\nu)$ derived in Eq. (20) in place of the total population size. Hence, the phase boundaries of inverse competitive exclusion for short period durations T are given by

$$\nu_l = \frac{\delta_2}{\mu_2} \cdot \frac{K_2 + S}{S}, \quad (21a)$$

$$\nu_u = \frac{\delta_1 \delta_2 (K_1 - K_2)}{\mu_2 \delta_1 K_1 - \mu_1 \delta_2 K_2}. \quad (21b)$$

The example above corresponds to the special case of zero resources during the period with resources absent in the chemostat model, $S' = 0$. The same arguments hold true for any other competing species model, in particular for the chemostat model with $S' > 0$. This method was used to calculate the phase boundaries at short period durations T in Figs. 5 and 6a-c.

3. Phase boundary on Coexistence

The results above were derived for the case where the period duration T is short compared to the time scales of growth, f_i^{-1} . This allowed to circumvent the nonlinearity of the dynamics by using a discrete map in order to analyse the characteristic population dynamics. However, it is precisely these nonlinear dynamics that lead to competitive exclusion in a time-independent system. Similarly, as the period duration T in a system with externally imposed time dependence becomes long enough such that a steady state is reached before the environment switches, the opportunist's short-term advantage vanishes and competitive exclusion can come into effect.

At what period duration T will this transition from inverse competitive exclusion to regular competitive exclusion occur? Inverse competitive exclusion holds as long as the gleaner cannot invade a prevailing opportunist population, i.e., as long as the average net growth rate

$$\langle f_1 \rangle(\nu) \Big|_{N=n_2^*(t)} = \frac{1}{T} \int_0^T dt f_1(n_2^*(t), t) < 0, \quad (22)$$

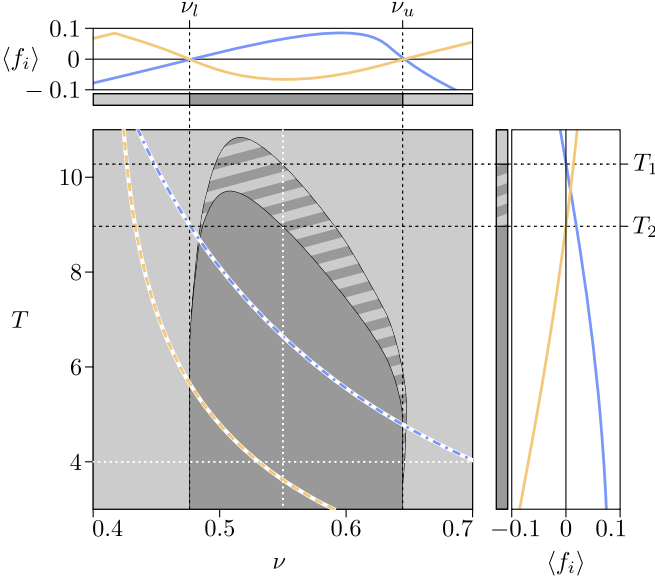


Figure 8. Simulated net growth rates $\langle f_i \rangle$ for the gleaner (n_1 , yellow or light gray) and the opportunist (n_2 , blue or dark gray), along two representative cutlines (dotted white) in the phase diagram of two-species competition. Bars next to the growth rate plots show the predicted outcome of the competition, based on the net growth rates: each species can survive if the net growth rate is positive, $\langle f_i \rangle > 0$. When both net growth rates are positive simultaneously, coexistence is predicted. Lines in the phase diagram show the estimated threshold period durations $\tilde{T}_1(\nu)$ (yellow, dashed) and $\tilde{T}_2(\nu)$ (blue, dash-dotted), providing results accurate within an order of magnitude.

where $n_2^*(t)$ is the asymptotic trajectory of the opportunist. Thus, a change in the qualitative dynamics occurs at a period duration T_1 at which $\langle f_1 \rangle|_{T_1} = 0$. Similarly, a threshold value T_2 can be obtained above which the opportunist cannot invade a gleaner population. For intermediate period durations $T_1 < T < T_2$, either species can invade the other, so that coexistence between these species is possible [Fig. 8].

However, since the asymptotic trajectories are in general not known, these phase boundaries cannot be calculated exactly. Instead, they can be estimated by approximating the asymptotic trajectories, or from the qualitative dynamics of the system. For the chemostat model as defined in Eq. (2), for example, the nonlinearities leading to coexistence between two species become relevant when the total population size approaches the steady state population size $S - \bar{K}_i$ of the dominant species. Thus, for any period duration T at which the total population size gets close to $S - \bar{K}_i$ before the environment changes, we expect the nonlinear interactions to be sufficiently relevant to favor the gleaner population.

To estimate the corresponding period duration T for each species independently, assume that the population size at the beginning of each period $t = k \cdot T$ is $n_i^*|_{S' > 0}$, as obtained from Eq. (20) for $S' > 0$. We furthermore

Figs. 2-5, 8	μ_1	2.0	δ_1	1.0	K_1	0.2
	μ_2	6.0	δ_2	1.0	K_2	2.0
	S	1.0	S'	0.1		
Fig. 6a-g	μ_1	1.8	δ_1	1.0	K_1	0.003
	μ_2	2.7	δ_2	1.0	K_2	0.018
	μ_3	4.5	δ_3	1.0	K_3	0.090
	S	1.0	S'	0.6		
Fig. 6h	μ_1	0.9	δ_1	0.5	K_1	0.003
	μ_2	1.1	δ_2	0.4	K_2	0.012
	μ_3	0.7	δ_3	0.1	K_3	0.130
	S	1.0	S'	0.4		
	T	10	ν	0.7		

Table I. Parameters used for numerically solving the ODEs and generating the plots.

assume the growth dynamics to be exponential, thereby ignoring the nonlinearities for this estimate. The period duration \tilde{T} at which the population reaches the steady state population size $S - \bar{K}_i$ is used as an estimate for threshold period duration:

$$S - \bar{K}_i = n_i^*|_{S'} \cdot \exp \left[\int_0^{\nu \tilde{T}_i} dt f_i(n_i^*|_{S'}, t) \right],$$

$$\rightarrow \quad \tilde{T}_i(\nu) = \frac{1}{\nu} \log \left(\frac{S - \bar{K}_i}{n_i^*|_{S'}} \right) \cdot \frac{1}{f_i(n_i^*|_{S'}, t)}. \quad (23)$$

Importantly, this estimate confirms that the inverse competitive exclusion can be expected only for $T \ll f_i^{-1}$.

E. Numerical solution of the ODE

To study the population dynamics in a specific system and to generate the figures, the differential equations in Eq. (2a) were solved numerically. Unless specified otherwise, the parameters stated in Table I were used throughout all numerical solutions. These parameters were chosen such that they fulfill the requirements for inverse competitive exclusion (two-species competition) and three-species coexistence (three-species competition) for a wide range of parameters ν and T , and with easily discernible visual features.

All phase diagrams were obtained by solving the differential equations numerically for each parameter combination (ν, T) separately. The numerical solver was terminated when one of the following criteria was met: (i) The population size of either species dropped below a threshold of $S \cdot 10^{-30}$ at the end of one period, i.e. at $t = k \cdot T$. (ii) A hard time limit of $t = 10^3 \cdot T$ was exceeded.

In order to classify the results, the population sizes at the final time step ($n_{i,k_{\max}}$) as well as the corresponding logarithmic population size change ($\log(n_{i,k_{\max}} - n_{i,k_{\max}-1})/T$) were used to bin a parameter combination as “competitive exclusion”, “inverse competitive exclusion” or “coexistence”. A species was considered

extinct if the population size was below the threshold of $n_{i,k_{\max}} < S \cdot 10^{-30}$. If both populations remained above this threshold until the solver stopped, the logarithmic population size change was used as a secondary criterion: a species was considered as extinct if $\log(n_{i,k_{\max}} - n_{i,k_{\max}-1})/T < -10^{-4}$. This threshold was chosen since it well predicted the outcome observed for larger T . If parameter combination was tagged as “competitive exclusion” if only the gleaner survived and “inverse competitive exclusion” if only the opportunist survived. If both populations survived, the parameter combination was tagged as “coexistence”.

For the invasion plots in Fig. 8, the system was simulated for one period with initial conditions $n_i(0) = 10^{-5}$, $n_j(0) = n_j^*(0) - n_i(0)$. Here, n_i is the invading population and n_j is the residing population, with its fixed trajectory $n_j^*(t)$. The net population change of the invading species after one period was used to determine the net growth rate, $\langle f_i \rangle = \log(n_i(T)/n_i(0))/T$.

F. Pairwise competition

In many-species ecosystem, an analytical study of the population dynamics is often difficult owed to the high-dimensionality and nonlinearity of the system. For competing species models where the interactions depend only on the total population size, however, it is sufficient to study pairwise interactions between species in order to understand the qualitative time evolution of the entire ecosystem. In the following, we justify this hypothesis.

Consider a general competing species model as defined in Eq. (3),

$$\frac{d}{dt}n_i(t) = n_i(t) \cdot f_i(N(t)), \quad (24a)$$

$$\frac{\partial}{\partial n_j} f_i(N) \leq 0, \quad (24b)$$

in a system hosting M distinct species. For simplicity, we assume a time-independent environment in the following, so that there is no explicit time dependence in the growth functions. Assume furthermore that this system is predominantly inhabited by one species, n_1 , with all other species contributing only marginally to the total population size, $n_1 \gg n_i$ with $i \in \{2, \dots, M\}$.

Now, consider the general case where the total population size is far from the dominant species’ steady state population size n_1^* . Then, since $\partial_t n_i(t) \sim n_i(t)$, this nonlinear growth ensures that the population size of n_1 can vary much more quickly than all other population sizes, $\partial_t n_1(t) \gg \partial_t n_i(t)$. Thus, the dominant species will quickly approach its steady state population size. Since this species contributes primarily to the total population size, the total population size will vary from this steady state population size only by a small amount, $N(t) = n_1^* + \Delta N(t)$. This allows to estimate the population dynamics for all species to lowest order:

$$\begin{aligned} \frac{d}{dt}n_1(t) &= n_1(t) \cdot f_1(n_1^* + \Delta N(t)) \\ &= n_1(t) \cdot \partial_n f_1(N) \Big|_{n_1^*} \Delta N(t) + \mathcal{O}(\Delta N^2), \end{aligned} \quad (25a)$$

$$\begin{aligned} \frac{d}{dt}n_i(t) &= n_i(t) \cdot f_i(n_1^* + \Delta N(t)) \\ &= n_i(t) \cdot f_i(n_1^*) + \mathcal{O}(n_i \cdot \Delta n). \end{aligned} \quad (25b)$$

Notably, since $\partial_N f_i \leq 0$ in the competing species model, the dominant population size changes such that the deviation Δn from the steady state population size is minimized. This ensures that the total population size remains close to $N(t) \approx n_1^*$ irrespective of the population changes of all other species, as long as n_1 is the dominant species. This shows that the growth rates of all subdominant populations is to lowest order determined by the steady state population size of the dominant species, n_1^* . Thus, in a many-species system, the population dynamics of all subdominant species are equivalent to a two-species system where the dominant species is the only competitor. In other words, the pairwise competition with the dominant species is sufficient to characterize the dynamics of all subdominant populations.

This reasoning can be extended to systems with an external time dependence. In these systems, a single population does not approach a fixed point, but rather an asymptotic trajectory $n_i^*(t)$. Following the same line of arguments, the total population size in such systems predominantly inhabited by one species $n_1(t) \gg n_i(t)$ is approximated by the asymptotic trajectory of this dominant species, $N(t) \approx n_1^*(t)$. This means that also in a time-dependent environment it is sufficient to consider pairwise competition to characterize the entire system’s population dynamics.